# A simple orbit-attitude coupled modelling method for large solar power satellites

Qingjun Li[a, c], Bo Wang[b], Zichen Deng[a*], Huajiang Ouyang[c], Yi Wei[d]

(a. Department of Engineering Mechanics, Northwestern Polytechnical University, Xi'an, Shaanxi, 710072, China)

(b. Qian Xuesen Laboratory of Space Technology, Beijing, 100094, China)

(c. School of Engineering, University of Liverpool, Liverpool, England, L69 3GH, United Kingdom)

(d. Department of Applied Mathematics, Northwestern Polytechnical University, Xi'an, Shaanxi, 710072, China)

**Abstract:** A simple modelling method is proposed to study the orbit-attitude coupled dynamics of large solar power satellites based on natural coordinate formulation. The generalized coordinates are composed of Cartesian coordinates of two points and Cartesian components of two unitary vectors instead of Euler angles and angular velocities, which is the reason for its simplicity. Firstly, in order to develop natural coordinate formulation to take gravitational force and gravity gradient torque of a rigid body into account, Taylor series expansion is adopted to approximate the gravitational potential energy. The equations of motion are constructed through constrained Hamilton's equations. Then, an energy- and constraint-conserving algorithm is presented to solve the differential-algebraic equations. Finally, the proposed method is applied to simulate the orbit-attitude coupled dynamics and control of a large solar power satellite considering gravity gradient torque and solar radiation pressure. This method is also applicable to dynamic modelling of other rigid multibody aerospace systems.

**Keywords:** Solar power satellite; Natural coordinate formulation; Gravity gradient torque; Solar radiation pressure; Differential-algebraic equations;

## 1. Introduction

The focus of this paper is to investigate very large solar power satellites (SPSs) that collect solar

[*] Corresponding author, Email address: dweifan@nwpu.edu.cn.

energy to generate electricity in space and then transmit it to the Earth. Due to the reducing resources and environmental problems of fossil fuel [1], SPSs have attracted much attention from scientists [2]. Since the first concept of SPS was proposed [3], many concepts have been put forward, such as 1979 SPS reference system [1], sail tower SPS [4], tethered SPS [5], integrated symmetrical concentrator (ISC) [6], and so on. The concept of ISC can avoid the use of slip rings and long distance power delivery that appear in other concepts [7]. The concept of ISC is that, by siting the primary reflectors at the ends of a long truss and reflecting solar radiation to the solar panel, solar power at high intensity is collected, and then the generated electricity is transmitted to the ground by transmitting antenna. Based on the concept of ISC, Japan Aerospace Exploration Agency (JAXA) has developed several concepts of SPS, such as 2001 JAXA reference model [8], 2002 JAXA reference model [8] and formation flying SPS model [9].

Since an SPS is a very large space system, its dynamics and control are of great importance. However, there are few investigations into the dynamics and control issues of SPSs [10]. McNally et al. [11] studied the orbit dynamics of SPSs in geosynchronous Laplace plane (GLP) orbit and geosynchronous equatorial orbit (GEO), and they found that SPSs located in GLP orbit required almost no fuel to maintain its orbit and could minimize the risk of debris, compared with SPSs in GEO. Wie and Roithmayr [12, 13] investigated the effects of perturbations on orbit and attitude dynamics of Abacus SPS, and they designed orbit and attitude controllers considering perturbations and system uncertainties using electric propulsion thrusters. Wu et al. [10] proposed a time-varying robust optimal control strategy and applied it to the attitude control of Abacus SPS. Liu et al. [14] studied the effects of fourth order gravitational force and torque on the dynamic response and control accuracy of the sail tower SPS. Fujii et al. [15, 16] investigated the vibration control algorithm for solar panels of tethered SPS by adjusting the tension of tethers, and they verified their method through experiments on the ground. Ishimura and Higuchi [17] studied the coupled dynamics of attitude motion and structural vibration of tethered SPS, and they found that the coupling phenomenon results from low stiffness of tethers and thermal deformation of solar panels. Senda and Goto [18] constructed a dynamic model of tethered SPS and proposed an attitude control method by geomagnetic force. Jin et al. [19, 20] studied the trajectory planning for SPSs with reflectors to obtain real-time Earth pointing and Sun pointing by rotating the truss and the reflectors cooperatively.

From the aforementioned review, the Euler angle representation was used to investigate simple single-rigid-body problems. For complicated rigid multibody systems, such as ISC and sail tower SPS, natural coordinate formulation (NCF) is an effective method to simplify the modelling process [21]. NCF uses two Cartesian coordinate points and two Cartesian unitary vectors as dependent generalized coordinates of a rigid body so that the modelling process is very easy to understand [22]. Meanwhile, by sharing the Cartesian coordinate points by contiguous bodies, NCF reduces the number of joint constraints [21, 23]. On the basis of NCF, zhao et al. [24] established the solar sails model and investigated the dynamic behavior of deployment. Based on the NCF, Liu et al. [25], constructed the dynamic model for rigid-flexible satellite system, and they [26] investigated the dynamics and control of a satellite-based robot with six arms. However, it is necessary to mention that, in the above works on NCF, the effect of gravity gradient torque was neglected. Gravity gradient torque is one of the main sources of attitude perturbations for SPSs [12], hence, it is necessary to be taken into account [14].

The objective of this paper is to develop NCF to take gravitational force as well as gravity gradient torque into consideration so that this simple modelling method is applicable to orbit-attitude coupled modelling of complicated SPSs. This paper is organized as follows. The orbit-attitude coupled modelling method for a rigid body is proposed in section 2. In section 3, an energy- and constraint-conserving algorithm for DAEs is presented. A simple example is carried out to validate the proposed modelling method and proposed numerical method in section 4. Section 5 presents dynamic modelling and attitude controller design for 2002 JAXA reference model of SPS. Simulation results are given and discussed in section 6 and conclusions are drawn in the last section.

## 2. Orbit-attitude coupled modelling method

This section presents the derivation of NCF to take gravitational force and gravity gradient torque of a rigid body into account, which begins with some basic concepts of NCF. In NCF, a rigid body is described in a global inertial coordinate system $O\text{-}XYZ$, as shown in Fig. 1. $\mathrm{P_i}$ and $\mathrm{P_j}$ are two fixed points of the rigid body. $\boldsymbol{e}$, $\boldsymbol{u}$ and $\boldsymbol{v}$ are orthogonal unit vectors connected to the rigid body. $\boldsymbol{r}_i$ and $\boldsymbol{r}_j$ are the vectors of global coordinates of $\mathrm{P_i}$ and $\mathrm{P_j}$. $l$ is the distance between $\mathrm{P_i}$ and $\mathrm{P_j}$. In order to describe the motion of a rigid body, $\boldsymbol{r}_i$, $\boldsymbol{r}_j$, $\boldsymbol{u}$ and $\boldsymbol{v}$ are selected as generalized coordinates

$$\boldsymbol{q}=\left[\boldsymbol{r}_i^{\mathrm{T}},\boldsymbol{r}_j^{\mathrm{T}},\boldsymbol{u}^{\mathrm{T}},\boldsymbol{v}^{\mathrm{T}}\right]^{\mathrm{T}}\in \mathrm{R}^{12}. \tag{1}$$

These generalized coordinates are dependent since there are only 6 degrees of freedom for a rigid body. They are subjected to the following constraints [21]

$$\begin{cases} \left(\boldsymbol{r}_j-\boldsymbol{r}_i\right)^{\mathrm{T}}\left(\boldsymbol{r}_j-\boldsymbol{r}_i\right)-l^2=0, \\ \boldsymbol{u}^{\mathrm{T}}\boldsymbol{u}-1=0, \\ \boldsymbol{v}^{\mathrm{T}}\boldsymbol{v}-1=0, \\ \left(\boldsymbol{r}_j-\boldsymbol{r}_i\right)^{\mathrm{T}}\boldsymbol{u}=0, \\ \left(\boldsymbol{r}_j-\boldsymbol{r}_i\right)^{\mathrm{T}}\boldsymbol{v}=0, \\ \boldsymbol{u}^{\mathrm{T}}\boldsymbol{v}=0, \end{cases} \tag{2}$$

which describe in sequence the distance between two points, the lengths of two vectors and the orthogonality between vectors. The above constraints are abbreviated as

$$\boldsymbol{g}(\boldsymbol{q})=\boldsymbol{0}\in \mathrm{R}^6. \tag{3}$$

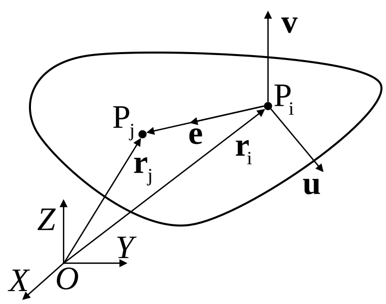


Fig. 1 NCF description of a rigid body

The equations of motion of the rigid body are constructed by constrained Hamilton's equations. Generally, there are two steps: firstly to obtain the constrained Hamiltonian function, and secondly to calculate the derivatives of the constrained Hamiltonian function with respect to generalized variables. The constrained Hamiltonian function of the rigid body is written as [27]

$$H=T(\dot{\boldsymbol{q}})+U(\boldsymbol{q})+\boldsymbol{\lambda}^{\mathrm{T}}\boldsymbol{g}(\boldsymbol{q})=\frac{1}{2}\dot{\boldsymbol{q}}^{\mathrm{T}}\boldsymbol{M}\dot{\boldsymbol{q}}+U(\boldsymbol{q})+\boldsymbol{\lambda}^{\mathrm{T}}\boldsymbol{g}(\boldsymbol{q}), \tag{4}$$

where $T(\dot{\boldsymbol{q}})$ is the kinetic energy, $\boldsymbol{M}$ is the mass matrix of the rigid body, $U(\boldsymbol{q})$ is the gravitational potential energy and $\boldsymbol{\lambda}\in \mathrm{R}^6$ is the vector of Lagrange multipliers. The mass matrix is calculated by [21]

$$\boldsymbol{M}=\begin{bmatrix} \left(m+\frac{I_x}{l^2}-\frac{2mx_G}{l}\right)\boldsymbol{I}_3 & \left(\frac{mx_G}{l}-\frac{I_x}{l^2}\right)\boldsymbol{I}_3 & \left(my_G-\frac{I_{xy}}{l}\right)\boldsymbol{I}_3 & \left(mz_G-\frac{I_{xz}}{l}\right)\boldsymbol{I}_3 \\ & \frac{I_x}{l^2}\boldsymbol{I}_3 & \frac{I_{xy}}{l}\boldsymbol{I}_3 & \frac{I_{xz}}{l}\boldsymbol{I}_3 \\ & \text{symmetric} & I_y\boldsymbol{I}_3 & I_{yz}\boldsymbol{I}_3 \\ & & & I_z\boldsymbol{I}_3 \end{bmatrix}, \tag{5}$$

where $\boldsymbol{I}_3 \in \mathrm{R}^{3\times3}$ is an identity matrix, $m$ is the mass of the rigid body, and $[x_G, y_G, z_G\ ]^{\mathrm{T}}$ is the coordinates of centre of mass in $\mathrm{P_i}$-$\boldsymbol{euv}$ coordinate system. $I_{xx}$, $I_{yy}$, and $I_{zz}$ are the moments of inertia with respect to $\mathrm{P_i}$-$\boldsymbol{euv}$, $I_{xy}$, $I_{yz}$ and $I_{xz}$ are the products of inertia with respect to $\mathrm{P_i}$-$\boldsymbol{euv}$. $I_x$, $I_y$, and $I_z$ are calculated as

$$\begin{bmatrix} I_x \\ I_y \\ I_z \end{bmatrix} = \frac{1}{2}\begin{bmatrix} -1 & 1 & 1 \\ 1 & -1 & 1 \\ 1 & 1 & -1 \end{bmatrix}\begin{bmatrix} I_{xx} \\ I_{yy} \\ I_{zz} \end{bmatrix}. \tag{6}$$

The gravitational potential energy in Eq. (4) is calculated as [28]

$$U(\boldsymbol{q}) = -\mu \int_V \frac{\rho}{\sqrt{\boldsymbol{r}^{\mathrm{T}}\boldsymbol{r}}}\mathrm{d}V = -\mu \int_V \rho f(\boldsymbol{r})\,\mathrm{d}V, \tag{7}$$

where $\boldsymbol{r}$ is the Cartesian coordinates of an arbitrary point in the rigid body, $f(\boldsymbol{r}) = 1/\sqrt{\boldsymbol{r}^{\mathrm{T}}\boldsymbol{r}}$ is a nonlinear function of $\boldsymbol{r}$, $\mu = 3.986 \times 10^{14}\ \mathrm{m^3 s^{-2}}$ is the standard gravitational parameter of the Earth, $\rho$ is the density of the rigid body, and $V$ is the volume of the rigid body. However, it is not easy to obtain $U(\boldsymbol{q})$ analytically. Wang and Xu employed Taylor series expansion to approximate the gravitational potential energy of a rigid body [28]. According to their results, both the lowest order of gravity gradient torque and second order of gravitational potential energy are expressed by the inertia matrix of the rigid body. Therefore, in order to take gravity gradient torque into account, a second-order Taylor series expansion is adopted to approximate $f(\boldsymbol{r})$ around the centre of mass $\boldsymbol{r}_0$, and the approximated gravitational potential energy is expressed by

$$U(\boldsymbol{q}) \approx \frac{-\mu}{2(\boldsymbol{r}_0{}^{\mathrm{T}}\boldsymbol{r}_0)^{5/2}}\left(d_{xx}\frac{I_x}{l^2} + d_{yy}I_y + d_{zz}I_z + d_{xy}\frac{I_{xy}}{l} + d_{xz}\frac{I_{xz}}{l} + d_{yz}I_{yz} + d_x m\frac{x_G}{l} + d_y m y_G + d_z m z_G + d_0 m\right), \tag{8}$$

where

$$\begin{cases} d_{xx} = h(\boldsymbol{r}_j - \boldsymbol{r}_i, \boldsymbol{r}_j - \boldsymbol{r}_i, \boldsymbol{r}_0), \\ d_{yy} = h(\boldsymbol{u}, \boldsymbol{u}, \boldsymbol{r}_0), \\ d_{zz} = h(\boldsymbol{v}, \boldsymbol{v}, \boldsymbol{r}_0), \\ d_{xy} = 2h(\boldsymbol{r}_j - \boldsymbol{r}_i, \boldsymbol{u}, \boldsymbol{r}_0), \\ d_{xz} = 2h(\boldsymbol{r}_j - \boldsymbol{r}_i, \boldsymbol{v}, \boldsymbol{r}_0), \\ d_{yz} = 2h(\boldsymbol{u}, \boldsymbol{v}, \boldsymbol{r}_0), \\ d_x = 2h(\boldsymbol{r}_j - \boldsymbol{r}_i, \boldsymbol{r}_i, \boldsymbol{r}_0) - 3h(\boldsymbol{r}_j - \boldsymbol{r}_i, \boldsymbol{r}_0, \boldsymbol{r}_0), \\ d_y = 2h(\boldsymbol{u}, \boldsymbol{r}_i, \boldsymbol{r}_0) - 3h(\boldsymbol{u}, \boldsymbol{r}_0, \boldsymbol{r}_0), \\ d_z = 2h(\boldsymbol{v}, \boldsymbol{r}_i, \boldsymbol{r}_0) - 3h(\boldsymbol{v}, \boldsymbol{r}_0, \boldsymbol{r}_0), \\ d_0 = h(\boldsymbol{r}_i, \boldsymbol{r}_i, \boldsymbol{r}_0) - 3h(\boldsymbol{r}_i, \boldsymbol{r}_0, \boldsymbol{r}_0) + 3h(\boldsymbol{r}_0, \boldsymbol{r}_0, \boldsymbol{r}_0), \end{cases} \tag{9}$$

and $h(\cdot,\cdot,\cdot)$ is a scalar function defined as

$$h(\boldsymbol{\alpha}, \boldsymbol{\beta}, \boldsymbol{\chi}) = 3(\boldsymbol{\alpha}^{\mathrm{T}}\boldsymbol{\chi})\boldsymbol{\beta}^{\mathrm{T}}\boldsymbol{\chi} - (\boldsymbol{\alpha}^{\mathrm{T}}\boldsymbol{\beta})\boldsymbol{\chi}^{\mathrm{T}}\boldsymbol{\chi}. \tag{10}$$

Now that the constrained Hamiltonian function is obtained, the second step is to calculate the derivatives of it. By introducing the generalized momenta vector [27]

$$\boldsymbol{p} = \frac{\partial T(\dot{\boldsymbol{q}})}{\partial \dot{\boldsymbol{q}}} = \boldsymbol{M}\dot{\boldsymbol{q}}, \tag{11}$$

Eq. (4) can be re-written as

$$H = \frac{1}{2}\boldsymbol{p}^{\mathrm{T}}\boldsymbol{M}^{-1}\boldsymbol{p} + U(\boldsymbol{q}) + \boldsymbol{\lambda}^{\mathrm{T}}\boldsymbol{g}(\boldsymbol{q}). \tag{12}$$

Both the generalized coordinates and generalized momenta are generalized variables of the equations of motion. By calculating the derivatives of Eq. (12) [27], the equations of motion are obtained:

$$\begin{cases} \dot{\boldsymbol{q}} = \frac{\partial H}{\partial \boldsymbol{p}} = \boldsymbol{M}^{-1}\boldsymbol{p}, \\ \dot{\boldsymbol{p}} = -\frac{\partial H}{\partial \boldsymbol{q}} = -\boldsymbol{g_q}^{\mathrm{T}}(\boldsymbol{q})\boldsymbol{\lambda} + \boldsymbol{f}_{\mathrm{g}}, \\ \boldsymbol{g}(\boldsymbol{q}) = \boldsymbol{0}, \end{cases} \tag{13}$$

where $\boldsymbol{g_q}(\boldsymbol{q}) \in \mathrm{R}^{6\times 12}$ is the Jacobian matrix of $\boldsymbol{g}(\boldsymbol{q})$, $\boldsymbol{f}_{\mathrm{g}} = -\partial U(\boldsymbol{q})/\partial \boldsymbol{q}$ is the vector of generalized gravitational force. If the term $\boldsymbol{f}_{\mathrm{g}}$ is ignored, the proposed method is reduced to NCF method.

It can be seen from Eq. (1) that the generalized coordinates of the proposed method consist of Cartesian coordinates of two points and the Cartesian components of two unit vectors, therefore it is easy to understand. The mass matrix (Eq. (5)) is a constant matrix, and the equations of motion (Eqs. (13)) are very simple. Furthermore, the proposed method avoids the singularity and additional body-fixed reference frame, compared with the most widely used Euler angle method.

## 3. Energy- and constraint-conserving algorithm

This section introduces a new method to solve the equations of motion numerically. The equations of motion obtained by NCF are differential-algebraic equations (DAEs). Eqs. (13) can be re-written as a more compact form

$$\begin{cases} \dot{\boldsymbol{x}} = \boldsymbol{f}(t, \boldsymbol{x}, \boldsymbol{\lambda}), \\ \boldsymbol{g}(\boldsymbol{x}) = \boldsymbol{0}, \end{cases} \tag{14}$$

where $\boldsymbol{x} = [\boldsymbol{q}^{\mathrm{T}}, \boldsymbol{p}^{\mathrm{T}}]^{\mathrm{T}} \in \mathrm{R}^{24}$ is the vector of state variables, and

$$\boldsymbol{f}(t, \boldsymbol{x}, \boldsymbol{\lambda}) = \begin{bmatrix} \boldsymbol{M}^{-1}\boldsymbol{p} \\ -\boldsymbol{g_q}^{\mathrm{T}}(\boldsymbol{q})\boldsymbol{\lambda} + \boldsymbol{f}_{\mathrm{g}} \end{bmatrix}. \tag{15}$$

One of the most important problems in solving DAEs is constraint violation, which means that the constraint equations are not satisfied strictly [29, 30]. There are many methods to deal with constraint violation, such as generalized α method [31], projection method [32] and energy- and constraint-conserving algorithm [33]. The energy- and constraint-conserving algorithm, which not only preserves the total energy and constraints of the constrained Hamiltonian systems but also has the characteristics of high accuracy and long-term stability, is suitable for long-time simulation of SPS. Based on the idea of literature [33], a new energy- and constraint-conserving algorithm is developed using Runge-Kutta method.

In order to solve Eqs. (14), the Runge-Kutta algorithm [34] is developed to discretize Eqs. (14) into the following nonlinear equations:

$$\begin{cases} \boldsymbol{x}_{n+1} = \boldsymbol{x}_n + \tau \sum_{i=1}^{s} b_i \boldsymbol{k}_i , \\ \boldsymbol{k}_i = \boldsymbol{f}\left(t_n + c_i\tau, \boldsymbol{x}_n + \tau \sum_{j=1}^{s} a_{ij}\boldsymbol{k}_j , \boldsymbol{\lambda}_n\right), i = 1,2,\cdots,s, \\ \boldsymbol{g}(\boldsymbol{x}_{n+1}) = \boldsymbol{0}, \end{cases} \tag{16}$$

where $\tau$ is the time step size, $\boldsymbol{b} = [b_1, b_2, \cdots, b_s]^{\mathrm{T}} \in \mathrm{R}^{s}$, $\boldsymbol{A} = \left[a_{ij}\right]_{s\times s} \in \mathrm{R}^{s\times s}$, and $c_i = \sum_{j=1}^{s} a_{ij}, i = 1,2,\cdots,s$ are the coefficients of Runge-Kutta method. In Eqs. (16), the unknowns are $\boldsymbol{x}_{n+1}$, $\boldsymbol{k}_i, i = 1,2,\cdots,s$, and $\boldsymbol{\lambda}_n$. The number of unknowns is equal to the number of equations so that Eqs. (16) can be solved by Newton-Raphson iteration. To improve the efficiency of the algorithm, one can substitute $\boldsymbol{x}_{n+1}$ into the constraint equations, and then Eqs. (16) can be divided into a linear part

$$\boldsymbol{x}_{n+1} = \boldsymbol{x}_n + \tau \sum_{i=1}^{s} b_i \boldsymbol{k}_i \tag{17}$$

and a nonlinear part

$$\begin{cases} \boldsymbol{k}_i = \boldsymbol{f}\left(t_n + c_i\tau, \boldsymbol{x}_n + \tau\sum_{j=1}^{s} a_{ij}\boldsymbol{k}_j, \boldsymbol{\lambda}_n\right), i = 1,2,\cdots,s, \\ \boldsymbol{g}\left(\boldsymbol{x}_n + \tau\sum_{i=1}^{s} b_i\boldsymbol{k}_i\right) = \boldsymbol{0}. \end{cases} \tag{18}$$

Consequently, the nonlinear equations (18) instead of (16) need to be solved at every step so that the efficiency is improved. A 2-stage, 4th order symplectic Runge-Kutta algorithm is adopted in this paper, and the coefficients are given as follows [34]:

$$\boldsymbol{A} = \begin{bmatrix} \frac{1}{4} & \frac{1}{4} - \frac{\sqrt{3}}{6} \\ \frac{1}{4} + \frac{\sqrt{3}}{6} & \frac{1}{4} \end{bmatrix}, \boldsymbol{b} = \left[\frac{1}{2}, \frac{1}{2}\right]. \tag{19}$$

Consequently, there are three steps to solve Eqs. (14):

Step 1: the initial values of Eqs. (18) are $\boldsymbol{k}_1 = \boldsymbol{k}_2 = \boldsymbol{0}$, $\boldsymbol{\lambda}_n = \boldsymbol{0}$;

Step 2: solve Eqs. (18) by Newton-Raphson iteration to obtain $\boldsymbol{k}_1$, $\boldsymbol{k}_2$, and $\boldsymbol{\lambda}_n$;

Step 3: $\boldsymbol{x}_{n+1} = \boldsymbol{x}_n + \frac{\tau}{2}\boldsymbol{k}_1 + \frac{\tau}{2}\boldsymbol{k}_2$, $n = n + 1$, go to Step 1.

## 4. Validation of the proposed modelling and numerical method

In order to validate the modelling method and the numerical method developed by the authors, the dynamic response of a rigid body (a disc) in space as a simple example is analysed, as shown in Fig. 2. In this example, the proposed modelling method and proposed numerical method are compared with the well-developed Euler angle method and Runge-Kutta method. The radius and thickness of the disc are all taken as 1 m. The orbital radius of the disc is $r_0 = 42{,}164$ km and the initial angular velocity of orbital motion is $\omega_0 = \sqrt{\mu/(r_0{}^3)}$. The initial angular velocity of the disc is $\omega_0 \times [0,1,1.1]^{\mathrm{T}}$.

Four cases are discussed as shown in Table 1. In Case 1, the gravity gradient torque is calculated on the base of Euler angle method (Chapter 3 of [35]), and the Runge-Kutta method [36] is used to solve the ordinary differential equations. The results of Case 1 are considered accurate results and the other cases are compared against Case 1, because the methods of Case 1 are the most widely used modelling method and numerical method. In Case 2, the simulation is carried out based on the proposed modelling method and proposed numerical algorithm. In Case 3, the gravity gradient torque is neglected, so the proposed modelling method is reduced to NCF method. In Case 4, the proposed modelling method is adopted, however, the equations are solved by the generalized α method [31]. Simulation results are depicted in Fig. 3 - Fig. 5. The error, relative energy error and constraint error are defined as

$$\begin{cases} Error = \boldsymbol{v}_{\mathrm{Case}\ k}(z) - \boldsymbol{v}_{\mathrm{Case}\ 1}(z), k = 2,3,4, \\ E_{\mathrm{error}} = \frac{E-E_0}{E_0}, \\ C_{\mathrm{error}} = \boldsymbol{u}^{\mathrm{T}}\boldsymbol{v}, \end{cases} \tag{20}$$

where $E$ is the total system energy of the disc, and $E_0$ is the initial value of $E$.

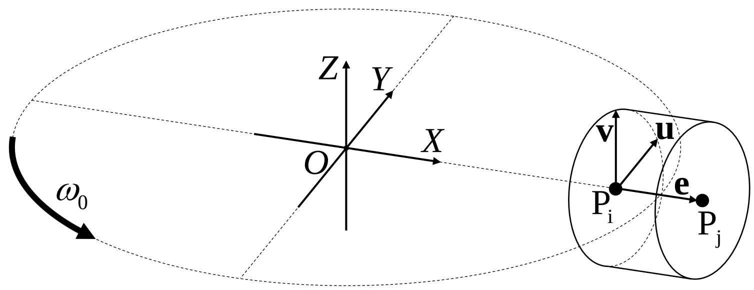


Fig. 2 A disc in space

Table 1. Four cases of simulation of a disc in space

| | Gravity gradient torque | Modelling method | Numerical method |
|---|---|---|---|
| Case 1 | Yes | Euler angles | Classical Runge-Kutta method |
| Case 2 | Yes | NCF | Energy- and constraint-conserving algorithm |
| Case 3 | No | NCF | Energy- and constraint-conserving algorithm |
| Case 4 | Yes | NCF | Generalized α method |

Fig. 3 shows the errors of $Z$ component of vector $\boldsymbol{v}$ compared with Case 1. From the results, one can easily find that the differences between Case 1 and Case 2 are very small, which indicates that the proposed modelling method is validated, and the gravity gradient torque of a space rigid body has been taken into account accurately. It also verifies that the proposed numerical method for DAEs produces accurate results in the simulation. From the errors of Case 3, it is found that the gravity gradient torque has a significant effect on the attitude dynamics of spacecraft and needs to be taken into account. The increasing errors of Case 4 indicate that generalized α method is not suitable for long-time simulation.

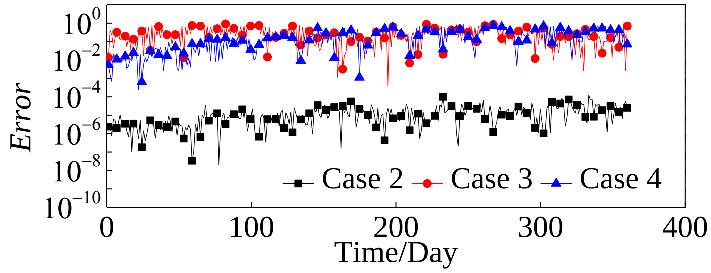


Fig. 3 Errors of $Z$ component of vector $\boldsymbol{v}$ compared with Case 1

Fig. 4 gives the relative errors of total system energy of Case 2 and Case 4. From the results, it is clearly found that the relative error of total system energy of the proposed numerical method is around $10^{-13}$ while the error of the generalized α method is above $10^{-3}$. Fig. 5 shows the error of constraint of Case 2, and it can be seen that the constraint is well satisfied. The conservation of total system energy using the proposed numerical method is due to the cofficients of Runge-Kutta method in Eqs. (19). The constraint is preserved precisely because the second equation in Eqs. (18) is well satisfied when solving Eqs. (18) by Newton-Raphson iteration method.

It can be concluded that the proposed modelling method and numerical method are validated. The following simulations of the SPS are carried out based on the proposed modelling method and numerical algorithm.

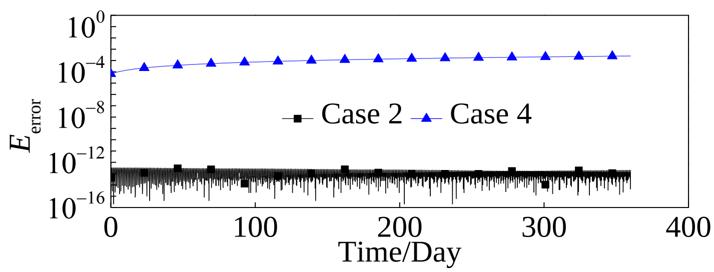


Fig. 4 Relative errors of total system energy of Case 2 and Case 4

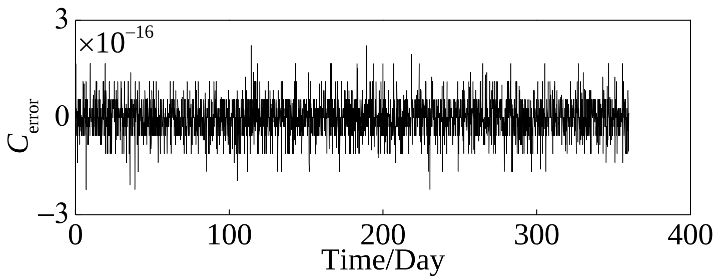


Fig. 5 Error of constraint of Case 2

# 5. Application on an SPS

Section 2 presents the modelling process of a single space rigid body. This section focuses on the dynamics and control of a rigid multibody aerospace system (an SPS). Firstly, a simplified three-rigid-body model is established based on the proposed modelling method. It will be shown that for rigid multibody aerospace system, the modelling process is also very simple and easy to understand. Then, an attitude controller is designed so that the transmitter can track the Earth and the primary reflectors can track the Sun synchronously. Finally, the effect of solar radiation pressure (SRP) is introduced, which is one of the most important attitude perturbations of SPSs.

## 5.1. Orbit-attitude coupled modelling

This sub-section presents the modelling process of a rigid multibody aerospace system, and the focus is given to 2002 JAXA reference model of SPS [8]. The difference between rigid multibody system and single rigid body is that there are additional constraints among rigid bodies in the rigid multibody system. Therefore, an important problem of modelling process of a rigid multibody aerospace system is how to deal with the additional constraints according to its characteristics. In the following paragraphs, the characteristics of 2002 JAXA reference model of SPS is given, and the modelling process is presented accordingly.

2002 JAXA reference model of SPS has two elliptic primary reflectors, two refracting lens, a truss and a transmitter, as illustrated in Fig. 6 and Fig. 7. The lens and the transmitter are fixed to the truss, and the primary reflectors can rotate around the truss to track the incident sunlight. The geometric and mass parameters are summarized in Table 2. $\mathrm{G_{ij}}$, $\mathrm{G_t}$, $\mathrm{G_{r1}}$, and $\mathrm{G_{r2}}$ are the centers of mass of the truss, the transmitter, refracting lens 1 and 2, respectively. The primary reflectors are considered to have a 45-degree and a 135-degree inclinations (to the truss axis) to reflect solar radiation to the refracting lens.

A global coordinate system *O-XYZ* is established as shown in Fig. 8. The origin is located at the center of the Earth. The *OZ* axis is along the rotational axis of the Earth and the *OX* axis points to the spring equinox at J2000. The *OY* axis can be determined by the right-hand rule.

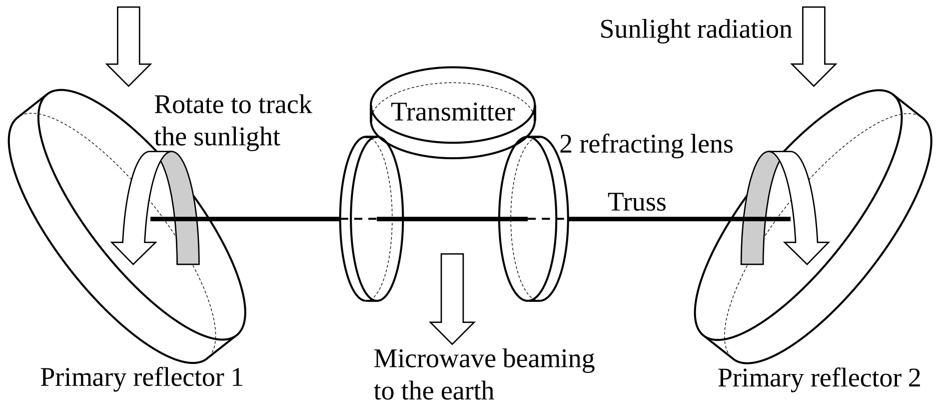


Fig. 6 2002 JAXA reference model of SPS

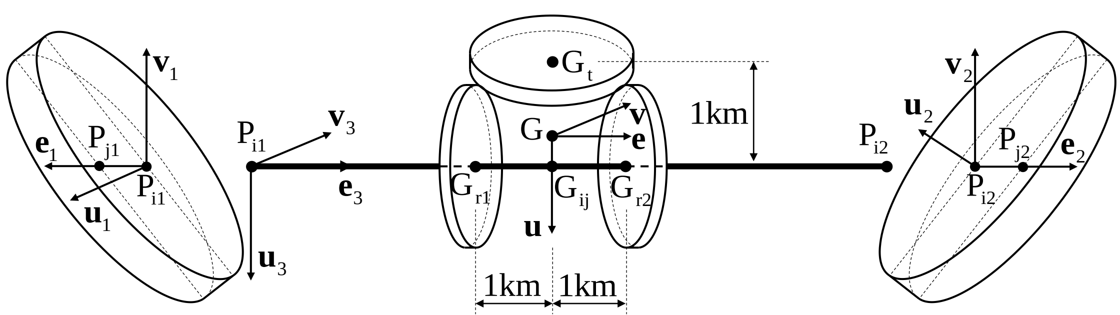


Fig. 7 Simplified three-rigid-body model of 2002 JAXA reference model of SPS (body 1: reflector 1; body 2: reflector 2; body 3: the truss with lens and transmitter)

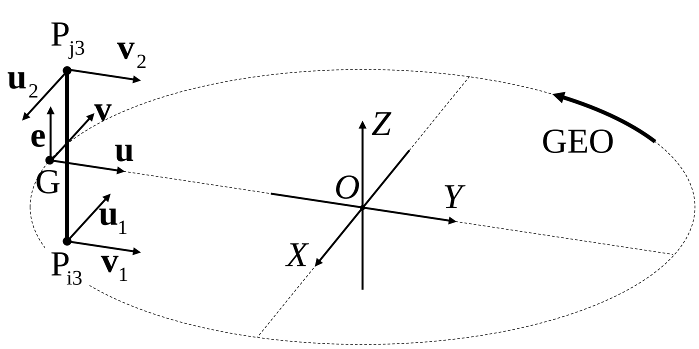


Fig. 8 Coordinate definition of motion (other components are not shown in the figure for simplicity)

Table 2. Geometric and mass parameters of 2002 JAXA reference model of SPS [8]

| Component | Length (m) | Diameter (m) | Weight (kg) |
|---|---|---|---|
| Truss | 6,000 | 100 m (Assumed) | 200,000 |
| Primary reflectors | 100 (Assumed) | 3,500 × 2,500 (Long and short axes) | 1,000,000 |
| Refracting lens | 50 (Assumed) | 2,000 | 400,000 |
| Transmitter | 50 (Assumed) | 2,000 | 7,000,000 |

The three-rigid-body model has 8 degrees of freedom: three translations, three rotations of the whole structure as one rigid object, and one relative rotational degree of freedom of each primary reflector. In Fig. 7, $\mathrm{P}_{\mathrm{i3}}$ and $\mathrm{P}_{\mathrm{j3}}$ are coincide with $\mathrm{P}_{\mathrm{i1}}$ and $\mathrm{P}_{\mathrm{i2}}$, respectively. $\boldsymbol{e}_1$ and $\boldsymbol{e}_2$ are collinear with $\boldsymbol{e}_3$. $\boldsymbol{u}_1$ and $\boldsymbol{u}_2$ coincide with minor axes of primary reflectors. $\boldsymbol{u}_3$ is the direction of the microwave beaming. Other vectors can be decided by the right-hand rule. In Fig. 7 and Fig. 8, G-$\boldsymbol{euv}$ is a local coordinate system, where G represents the center of mass of the whole SPS, $\boldsymbol{e}$, $\boldsymbol{u}$ and $\boldsymbol{v}$ axes are parallel to $\boldsymbol{e}_3$, $\boldsymbol{u}_3$ and $\boldsymbol{v}_3$ axes respectively. The coordinates of each rigid body is defined as

$$\boldsymbol{q}_k = \left[\boldsymbol{r}_{ik}{}^{\mathrm{T}}, \boldsymbol{r}_{jk}{}^{\mathrm{T}}, \boldsymbol{u}_k{}^{\mathrm{T}}, \boldsymbol{v}_k{}^{\mathrm{T}}\right]^{\mathrm{T}}, k = 1,2,3. \tag{21}$$

Apparently, there are 6 internal constraints for each rigid body (see Eqs. (2)). Apart from these constraints, there are 6 linear constraints and 4 nonlinear constraints among three bodies, described by the following equations:

$$\begin{cases} \boldsymbol{r}_{i1} - \boldsymbol{r}_{i3} = \boldsymbol{0}, \\ \boldsymbol{r}_{i2} - \boldsymbol{r}_{j3} = \boldsymbol{0}, \\ (\boldsymbol{r}_{i1} - \boldsymbol{r}_{i2})^{\mathrm{T}}\boldsymbol{u}_1 = 0, \\ (\boldsymbol{r}_{i1} - \boldsymbol{r}_{i2})^{\mathrm{T}}\boldsymbol{v}_1 = 0, \\ (\boldsymbol{r}_{i1} - \boldsymbol{r}_{i2})^{\mathrm{T}}\boldsymbol{u}_2 = 0, \\ (\boldsymbol{r}_{i1} - \boldsymbol{r}_{i2})^{\mathrm{T}}\boldsymbol{v}_2 = 0, \end{cases} \tag{22}$$

which restrict the relative translation and rotation among three bodies. In practice, the linear constraints can be eliminated to improve simulation efficiency. Eventually, $\boldsymbol{r}_{i3}$ and $\boldsymbol{r}_{j3}$ can be replaced by $\boldsymbol{r}_{i1}$ and $\boldsymbol{r}_{i2}$ respectively, and the generalized coordinates of the three-rigid-body model are chosen as

$$\boldsymbol{q} = \left[\boldsymbol{r}_{i1}{}^{\mathrm{T}}, \boldsymbol{r}_{j1}{}^{\mathrm{T}}, \boldsymbol{u}_1{}^{\mathrm{T}}, \boldsymbol{v}_1{}^{\mathrm{T}}, \boldsymbol{r}_{i2}{}^{\mathrm{T}}, \boldsymbol{r}_{j2}{}^{\mathrm{T}}, \boldsymbol{u}_2{}^{\mathrm{T}}, \boldsymbol{v}_2{}^{\mathrm{T}}, \boldsymbol{u}_3{}^{\mathrm{T}}, \boldsymbol{v}_3{}^{\mathrm{T}}\right]^{\mathrm{T}} \in \mathrm{R}^{30}. \tag{23}$$

Then, the nonlinear constraints of Eqs. (22) and the internal constraints of each rigid body are denoted concisely as

$$\boldsymbol{g}(\boldsymbol{q})=\mathbf{0} \in \mathrm{R}^{22}. \tag{24}$$

It is seen that the linear constraints can be eliminated to reduce the number of generalized coordinates and improve simulation efficiency. Alternatively, one may prefer not to eliminate the linear constraints to further simplify the modelling process, despite of simulation efficiency.

The equations of motion of the three-rigid-body model are also derived by constrained Hamilton’s equation. Both the kinetic energy and the gravitational potential energy of the system can be calculated by summing those of each rigid body. Therefore, the constrained Hamiltonian function of the three-rigid-body model can be written as [27]

$$H = T(\dot{\boldsymbol{q}})+U(\boldsymbol{q})+\boldsymbol{\lambda}^{\mathrm{T}}\boldsymbol{g}(\boldsymbol{q}) = \sum_{k=1}^{3} T_k(\dot{\boldsymbol{q}}_k) + \sum_{k=1}^{3} U_k(\boldsymbol{q}_k) + \boldsymbol{\lambda}^{\mathrm{T}}\boldsymbol{g}(\boldsymbol{q}), \tag{25}$$

where $\boldsymbol{\lambda} \in \mathrm{R}^{22}$ is the vector of Lagrange multipliers, $T(\dot{\boldsymbol{q}})$ is the kinetic energy of the system and $U(\boldsymbol{q})$ is the gravitational potential energy of the system. The expression of $U_k(\boldsymbol{q}_k)$ is shown in Eq. (8), and the mass matrix of each rigid body is given in Eq. (5). By replacing $\boldsymbol{r}_{i3}$ and $\boldsymbol{r}_{j3}$ with $\boldsymbol{r}_{i1}$ and $\boldsymbol{r}_{i2}$, the kinetic energy of the system can be written as

$$T(\dot{\boldsymbol{q}}) = \frac{1}{2}\dot{\boldsymbol{q}}^{\mathrm{T}}\boldsymbol{M}\dot{\boldsymbol{q}}, \tag{26}$$

where $\boldsymbol{M} \in \mathrm{R}^{30\times 30}$ is the constant mass matrix of the system. By using the constrained Hamilton’s equations [27], the equations of motion are obtained:

$$\begin{cases} \dot{\boldsymbol{q}} = \boldsymbol{M}^{-1}\boldsymbol{p}, \\ \dot{\boldsymbol{p}} = -\boldsymbol{g_q}^{\mathrm{T}}(\boldsymbol{q})\lambda + \boldsymbol{f}_{\mathrm{g}} + \boldsymbol{f}_{\mathrm{d}} + \boldsymbol{f}_{\mathrm{c}}, \\ \boldsymbol{g}(\boldsymbol{q}) = \mathbf{0}, \end{cases} \tag{27}$$

where $\boldsymbol{g_q}(\boldsymbol{q}) \in \mathrm{R}^{22\times 30}$ is the Jacobian matrix of $\boldsymbol{g}(\boldsymbol{q})$, $\boldsymbol{f}_{\mathrm{g}} = -\,\partial U(\boldsymbol{q})/\partial \boldsymbol{q}$, $\boldsymbol{f}_{\mathrm{d}}$ and $\boldsymbol{f}_{\mathrm{c}}$ are the vectors of generalized gravitational force, disturbing force, and control force respectively. $\boldsymbol{f}_{\mathrm{d}}$ and $\boldsymbol{f}_{\mathrm{c}}$ are obtained by the principle of virtual work. The mass matrix and the vector of generalized external force of the three-rigid-body model can be assembled from those of each rigid body.

### 5.2. Attitude controller design

The SPS needs to track the Earth and the Sun synchronously while it travels on GEO. In this sub-section, a proportional-derivative (PD) controller is designed for Earth-tracking and Sun-tracking control of the SPS. In order to describe the attitude of the SPS, a 3-1-2 sequence of Euler angle representation of G-$\boldsymbol{euv}$ (denoted by $\psi$ for $\boldsymbol{v}$ axis, $\varphi$ for $\boldsymbol{e}$ axis, and $\theta$ for $\boldsymbol{u}$ axis) is adopted. The initial orientations of $\boldsymbol{e}$, $\boldsymbol{u}$, and $\boldsymbol{v}$ are parallel to *OX*, *OY*, and *OZ* axes respectively.

In this paper, NCF is used to model the SPS, and Euler angle representation is adopted to design an attitude controller for the SPS. The relationship between NCF and Euler angles can be found through the mathematical expression of attitude matrix. The attitude matrix of Euler angle method is given by (Chapter 2 of [35])

$$\boldsymbol{A}=\begin{bmatrix}\cos\psi\cos\theta-\sin\psi\sin\varphi\sin\theta & \sin\psi\cos\theta+\cos\psi\sin\varphi\sin\theta & -\cos\varphi\sin\theta\\ -\sin\psi\cos\varphi & \cos\psi\cos\varphi & \sin\varphi\\ \cos\psi\sin\theta+\sin\psi\sin\varphi\cos\theta & \sin\psi\sin\theta-\cos\psi\sin\varphi\cos\theta & \cos\varphi\cos\theta\end{bmatrix}. \tag{28}$$

On the other hand, attitude matrix can also be written as [23]

$$\boldsymbol{A}_{\mathrm{m}}=[\boldsymbol{e}_3,\boldsymbol{u}_3,\boldsymbol{v}_3]^{\mathrm{T}}. \tag{29}$$

By comparing Eq. (28) with Eq. (29), the Euler angles can be expressed by $\boldsymbol{e}_3$, $\boldsymbol{u}_3$, and $\boldsymbol{v}_3$.

The primary reflectors need to track the Sun to collect solar power in space, meanwhile the transmitter needs to track the Earth to transmit power to the ground, as demonstrated in Fig. 9. The objective of the attitude control can be represented by the geometric relationship as

$$\begin{cases}\boldsymbol{e}_3=[0,0,1]^{\mathrm{T}},\\ \boldsymbol{u}_3=\boldsymbol{u}_{\mathrm{Earth}},\\ {\boldsymbol{u}_1}^{\mathrm{T}}\boldsymbol{u}_{\mathrm{Sun}}={\boldsymbol{u}_1}^{\mathrm{T}}\boldsymbol{u}_{\mathrm{Sun}}=0,\end{cases} \tag{30}$$

where $\boldsymbol{u}_{\mathrm{Earth}}$ is a unit vector from point G to point O and $\boldsymbol{u}_{\mathrm{Sun}}$ is a unit vector from point G to the Sun. Because the SPS travels on GEO, $\boldsymbol{u}_{\mathrm{Earth}}$ and $\boldsymbol{u}_{\mathrm{Sun}}$ can be simply expressed by

$$\begin{cases}\boldsymbol{u}_{\mathrm{Earth}}=[-\sin(\omega_{\mathrm{Earth}}t),\cos(\omega_{\mathrm{Earth}}t),0]^{\mathrm{T}},\\ \boldsymbol{u}_{\mathrm{Sun}}=[-\sin(\omega_{\mathrm{Sun}}t),\cos(\gamma)\cos(\omega_{\mathrm{Sun}}t),\sin(\gamma)\cos(\omega_{\mathrm{Sun}}t)]^{\mathrm{T}},\end{cases} \tag{31}$$

where $\omega_{\mathrm{Earth}}=2\pi/(23\times3600+56\times60+4)$ is the angular velocity of the Earth, $\omega_{\mathrm{Sun}}=\omega_{\mathrm{Earth}}/365.25$, $\gamma=23^{\circ}26'$ is obliquity of the ecliptic. By solving Eqs. (30) and Eqs. (22), the planed value of $\boldsymbol{e}_3$, $\boldsymbol{u}_3$, and $\boldsymbol{v}_3$ are obtained, and then the planed Euler angles can be obtained by comparing Eq. (28) with Eq. (29).

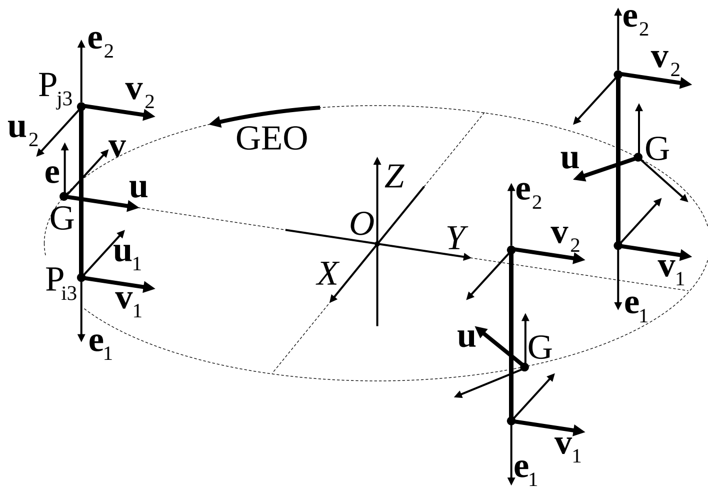


Fig. 9 Simple demonstration of Earth-tracking and Sun-tracking attitude

Fig. 10 shows the results of planed Euler angles of the SPS. From the results, one can easily find that $\psi_{\text{Planned}}$ increase linearly with time, $\varphi_{\text{Planned}}$ remains zero and $\theta_{\text{Planned}}$ remains $\pi/2$. The angular errors of $\psi$, $\varphi$ and $\theta$ are denoted as $e_\psi$, $e_\varphi$ and $e_\theta$, respectively. Synchronously, bodies 1 and 2 can rotate around the truss so that $\boldsymbol{v}_1$ and $\boldsymbol{v}_2$ can point to $\boldsymbol{u}_{\text{Sun}}$ direction. The error of attitude angle of body 1 (denoted by $e_1$) is defined in Fig. 11, where $\boldsymbol{u}'_{\text{Sun}}$ is the projection of $\boldsymbol{u}_{\text{Sun}}$ to P$_{\text{i1}}$-$\boldsymbol{u}_1\boldsymbol{v}_1$ plane. $e_2$ is defined similarly.

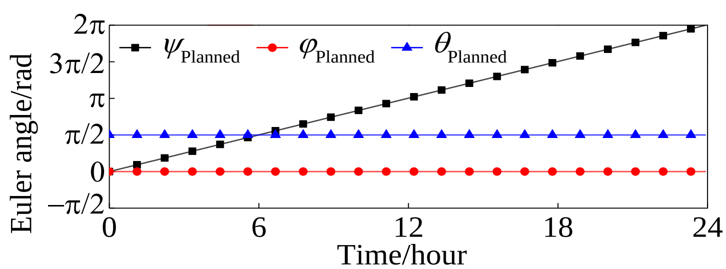


Fig. 10 Results of trajectory planning for body 3

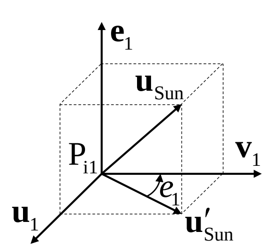

Fig. 11 Definition of attitude angle error of body 1

In order to track the Earth and the Sun synchronously, a simple PD controller [37] is designed as shown in Fig. 12. This PD controller is applied identically to $e_\psi$, $e_\varphi$, $e_\theta$, $e_1$ and $e_2$, therefore the subscripts are neglected for simplicity. Therefore, the output control moment of the PD controller is

$$M' = K_\mathrm{p}e + K_\mathrm{d}\dot{e}, \tag{32}$$

where $K_\mathrm{p}$ and $K_\mathrm{d}$ are proportional and derivative gains respectively.

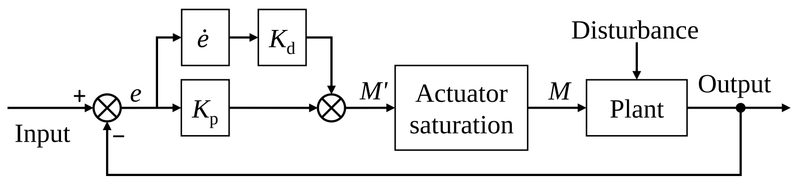


Fig. 12 Structure of attitude controller

In engineering applications, the output of an actuator is always limited to a specific maximum value. This phenomenon is termed actuator saturation. Under this practical consideration, a saturation function is employed to simulate the actuator saturation:

$$M = \begin{cases} -M_\mathrm{max}, & M' < -M_\mathrm{max}, \\ M', & -M_\mathrm{max} < M' < M_\mathrm{max}, \\ M_\mathrm{max}, & M_\mathrm{max} < M', \end{cases} \tag{33}$$

where $M_\mathrm{max}$ is the upper bound of actuator output. The upper bound should be determined through simulations so that it is known how big moments the actuators need to provide to track the planned attitude. At the same time, it should not be so large that the abilities of actuators are underutilized.

### 5.3. Solar radiation pressure (SRP)

Gravity gradient torque, SRP and the reactive force of microwave beaming are considered as three main sources of disturbing torques for SPS [12]. The gravity gradient torque has been taken into account by using the proposed formulation of gravitational potential energy. In addition, the direction of microwave beaming, which is $\boldsymbol{u}_3$ direction, passes through the centre of mass of the SPS. Consequently, the torque generated by reactive force of microwave beaming can be neglected. Thus, the main perturbation of attitude motion of the SPS is SRP.

The SRP force of a flat surface can be expressed as [12]

$$\boldsymbol{F}_\mathrm{s} = P_\mathrm{s}A(\boldsymbol{n}\cdot\boldsymbol{u}_\mathrm{Sun})\left\{(\rho_\mathrm{a}+\rho_\mathrm{d})\boldsymbol{u}_\mathrm{Sun} + \left[2\rho_\mathrm{s}(\boldsymbol{n}\cdot\boldsymbol{u}_\mathrm{Sun}) - \frac{2}{3}\rho_\mathrm{d}\right]\boldsymbol{n}\right\}, \tag{34}$$

where $P_{\mathrm{s}} = 4.5 \times 10^{6}\ N \cdot m^{-2}$ is the SRP constant, $A$ is the area of the flat surface, $\boldsymbol{n}$ is the normal vector of the surface and points into the surface, $\rho_{\mathrm{s}}$, $\rho_{\mathrm{d}}$, and $\rho_{\mathrm{a}}$ are coefficients of specular reflection, diffuse reflection, and absorption. The primary reflectors are assumed to be ideal mirrors with $\rho_{\mathrm{s}} = 1, \rho_{\mathrm{d}} = \rho_{\mathrm{a}} = 0$. For other components, the coefficients are considered to be $\rho_{\mathrm{s}} = \rho_{\mathrm{d}} = 0, \rho_{\mathrm{a}} = 1$. For the primary reflector 1, $\boldsymbol{n} = \sqrt{2}\,(\boldsymbol{e}_1 - \boldsymbol{v}_1)/2$. According to Eq. (34) and the parameters in Table 2, the SRP force of primary reflector 1 is

$$\boldsymbol{F}_{\mathrm{s,reflector1}} = 2P_{\mathrm{s}}A(\boldsymbol{n} \cdot \boldsymbol{u}_{\mathrm{Sun}})^2\boldsymbol{n} \approx \boldsymbol{61.8}(\boldsymbol{n} \cdot \boldsymbol{u}_{\mathrm{Sun}})^2\boldsymbol{n}. \tag{35}$$

According to Eqs. (31) and the planed attitude of the SPS, the maximum value of the SRP force of a primary is 53.5 N. The SRP force would produce a large torque ($10^4 \sim 10^5 \mathrm{N} \cdot \mathrm{m}$) on the SPS because the distance between the centre of pressure and the centre of mass of the system would reach the magnitude of kilometer.

## 6. Simulation results

The effects of gravity gradient torque and SRP on the orbit-attitude coupled dynamics of the SPS are presented in this section. The initial position and orientation of 2002 JAXA reference model of SPS in all cases are shown in Fig. 8. The system travels on GEO initially, and the initial angular velocities in $Z$ direction are all $\omega_{\mathrm{Earth}}$ for three bodies. SRP forces of all components are calculated by Eq. (34). To include 20% of uncertain offset between centers of mass and centers of pressure, the local coordinates of centers of pressure of primary reflectors 1 and 2 are assumed to be $[250{,}100{,}200]^{\mathrm{T}}$ and $[230, -150{,}190]^{\mathrm{T}}$ in $\mathrm{P_{i1}}$-$\boldsymbol{e}_1\boldsymbol{u}_1\boldsymbol{v}_1$ and $\mathrm{P_{i2}}$-$\boldsymbol{e}_2\boldsymbol{u}_2\boldsymbol{v}_2$ respectively. The centers of pressure of other components are assumed to coincide with their centers of mass.

Five cases are summarized in Table 3. The proposed method is used to establish the dynamic model of the SPS in Case 5 - Case 8, while the SPS is treated as a particle in Case 9. In Case 9, the attitude of the SPS is considered to be well-controlled.

Table 3. Five cases of simulation

| | Modelling method | SRP | Attitude controller |
|---|---|---|---|
| Case 5 | Proposed method | No | No |
| Case 6 | Proposed method | No | Yes |
| Case 7 | Proposed method | Yes | No |
| Case 8 | Proposed method | Yes | Yes |

| | | | |
|---|---|---|---|
| Case 9 | Particle | Yes | - |

### 6.1. Effects of gravity gradient torque

The effects of gravity gradient torque are studied by comparing Case 5 and Case 6. The relative errors of energy and the constraint error of Case 5 are illustrated in Fig. 13 and Fig. 14 to validate the simulation. They are defined as

$$\begin{cases} E_{\mathrm{SPS,error}} = \frac{E-E_0}{E_0}, \\ C_{\mathrm{SPS,error}} = \boldsymbol{u}_3{}^{\mathrm{T}}\boldsymbol{v}_3, \end{cases} \tag{36}$$

where $E$ is the total energy of the system, and $E_0$ is the initial value of $E$. It can be seen from Fig. 13 that the total relative errors of energy of Case 5 remains below $10^{-8}$. It means that when SRP and control force are not considered, the total energy of the system remains a constant. Fig. 14 indicates that the constraints of the system are well preserved in long-time simulation.

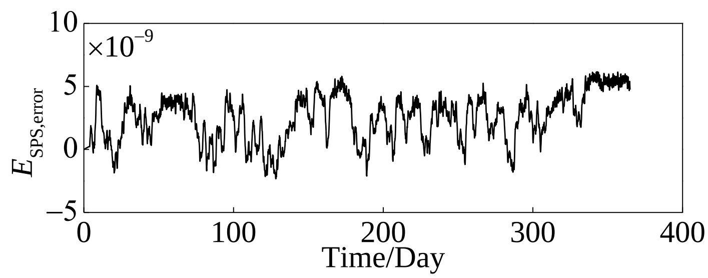


Fig. 13 Relative errors of energy of the three-rigid-body model (Case 5)

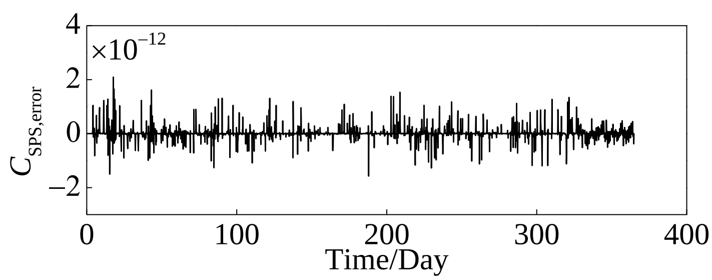


Fig. 14 Constraint errors of the three-rigid-body model (Case 5)

The errors of $\varphi$, the errors of primary reflector 1 and the control moments of primary reflector 1 are shown in Fig. 15, Fig. 16 and Fig. 17, respectively. It can be seen that when the attitude of the SPS is not controlled (Case 5), the Earth-pointing error remains zero in the first three days but increase greatly during the fourth day. The Sun-pointing error rises from the beginning of the simulation and reaches around 0.2 rad at the end. For Case 6, the Earth-pointing and Sun-pointing errors remain almost zero during the simulation. The control moment of primary reflector 1 oscillates periodically. The period of the control moment is about 12 hours, and the magnitude is about 56 N · m.

This simulation suggests that the initial attitude of the SPS is equilibrium due to its symmetry. However, the equilibrium is unstable under the disturbance of gravity gradient torque. Therefore attitude controller is significant to maintain the Earth-pointing stability and accuracy. On the other hand, periodic control moments on primary reflectors are required to counteract the effect of gravity gradient torque.

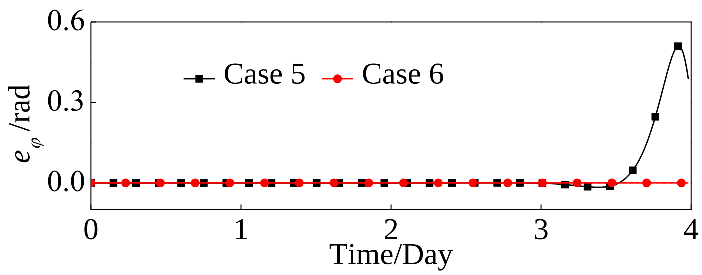


Fig. 15 Errors of $\varphi$ (Earth-pointing errors)

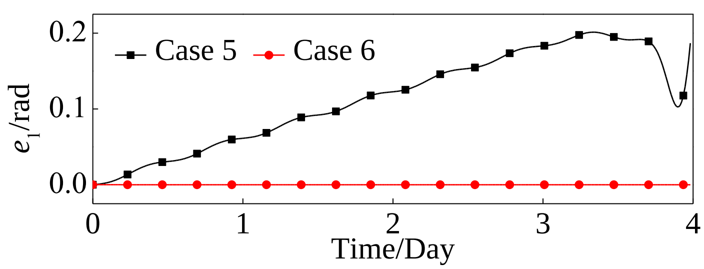


Fig. 16 Errors of primary reflector 1 (Sun-pointing errors)

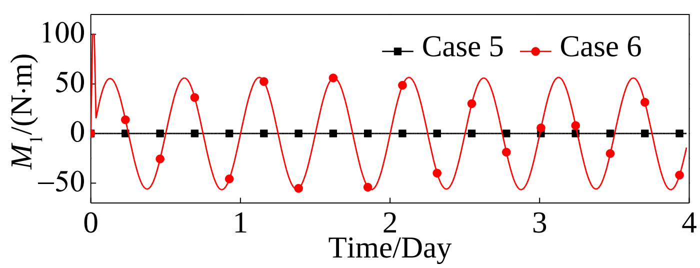


Fig. 17 Control moments of primary reflector 1 (Sun-pointing control moments)

## 6.2. Effects of SRP

This sub-section studies the effects of SRP on the orbital motion and attitude motion of the SPS. The orbital motion of the SPS can be represented by the orbital motion of its centre of mass

(Point G in Fig. 7). Based on the theory of two-body problem (Chapter 2 of [38]), the eccentricity of Point G can be expressed by the position vector and velocity vector of Point G.

Fig. 18 shows the orbital eccentricity of the SPS in one-year simulation. It can be found that the orbital eccentricity of Case 5 remains zero during the simulation, because SRP is not considered in Case 5. In Case 7- Case 9, the eccentricity of the SPS increases in the first half year and then decreases to about zero at the end of the year. The results of Case 8 and Case 9 are slightly different. The reason is that the attitude errors of Case 9 are considered to be zero while in Case 8 the attitude errors actually vibrate in a small range (see Fig. 19). The magnitude of eccentricity of Case 7 is lower than that of Case 8, because the attitude of Case 7 is not controlled and consequently cannot capture as much solar radiation as Case 8. The good agreement between Case 8 and Case 9 indicates that NCF method can predict the orbit of rigid multibody systems properly. It can also be concluded that the attitude of the SPS has considerable influence on its orbit when SRP is taken into account.

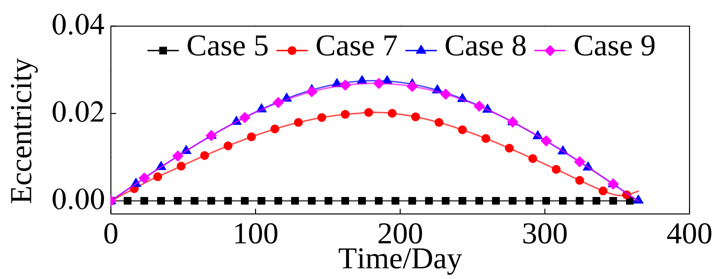


Fig. 18 Orbital eccentricity of the SPS

By comparing the control results of Case 6 and Case 8 in Fig. 19 and Fig. 20, we can find that SRP has a great influence on Earth-pointing control of 2002 JAXA reference model of SPS. SRP produces periodic Earth-pointing errors and necessitates large periodic control moments to counteract the disturbance of SRP. Although the control errors of Case 8 are below $10^{-3}$ rad (less than 0.1 degree), they are highly dependent on the gains of the controller. In other words, if the gains of PD controller were not chosen appropriately, the errors would rise. Therefore, the Earth-pointing controller should be further investigated to enhance Earth-pointing accuracy and reliability.

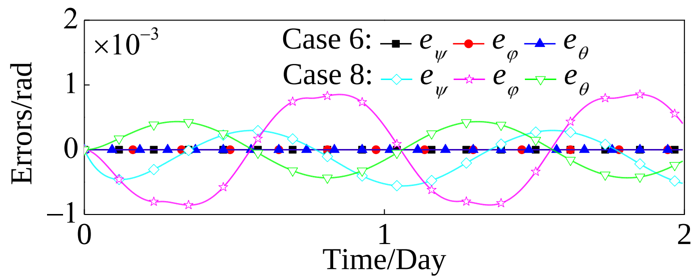


Fig. 19 Errors of $\psi$, $\varphi$ and $\theta$ (Earth-pointing errors)

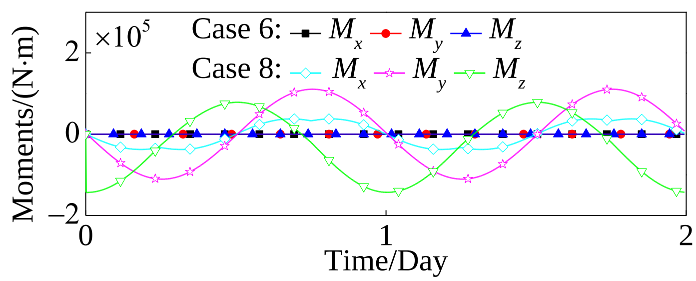


Fig. 20 Control moments of body 3 (Earth-pointing control moments)

The Sun-pointing control errors and control moments are presented in Fig. 21 and Fig. 22. It can be found that the control errors of primary reflectors in Case 8 increase significantly at the beginning of the simulation and then remain steady with a small fluctuation. The control errors in Case 6 keep fluctuating in a small value during the simulation. The control moments experience similar variations. The magnitude of control moment is determined by the magnitude of SRP torque, which can be further attributed to the offset between centre of mass and centre of pressure. It can be concluded that SRP generates a steady Sun-pointing error by exerting steady torques on primary reflectors. The torques is steady because the primary reflectors steadily point to the sun, and thus the SRP force and the offset between the centre of pressure and the centre of mass of the primary reflectors remain steady.

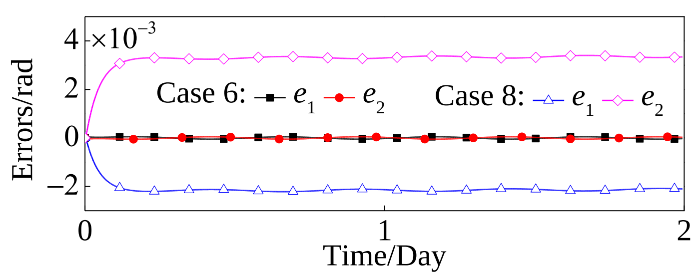


Fig. 21 Errors of primary reflector 1 and primary reflector 2 (Sun-pointing errors)

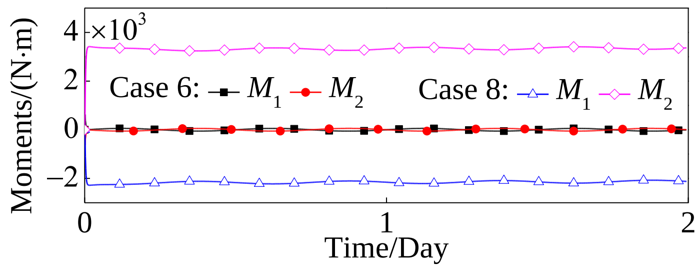


Fig. 22 Control moments of primary reflector 1 and primary reflector 2 (Sun-pointing control moments)

## 7. Conclusion

A simple method is proposed for orbit-attitude coupled modelling of large solar power satellite (SPS) based on natural coordinate formulation (NCF). An energy- and constraint-conserving algorithm is then presented to solve the differential-algebraic equations. Then, a simple example is carried out to show the validity of the proposed method. Finally, based on the proposed modelling method and numerical method, the orbit-attitude coupled model of 2002 JAXA reference model of SPS is constructed. According to simulation results, the Earth-pointing attitude of the SPS is an unstable equilibrium state under the disturbance of gravity gradient torque. Besides, periodic control moments on primary reflectors are required to counteract the effect of gravity gradient torque. On the other hand, solar radiation pressure (SRP) produces periodic Earth-pointing control errors and steady Sun-pointing control errors under proportional-derivative controller. Furthermore, it is found that the effect of SRP on orbital eccentricity of the SPS is dependent on its attitude, which necessitates the orbit-attitude coupled modelling of large SPS.

The proposed modelling method is an extension of NCF to consider gravitational force and gravity gradient torque for rigid multibody aerospace systems. Compared with Euler angle method, the proposed modeling method is simpler to use and easier to understand, because the generalized coordinates of the proposed method are all Cartesian coordinates in a global coordinate system. The proposed modelling method is also applicable to the simulation of other rigid multibody aerospace system, such as space robots, satellite rendezvous and docking, and on-orbit construction. Future works can be addressed to consider the effects of other space perturbations. On the other hand, the attitude controller of the SPS can be developed to deal with steady errors as well as periodic errors.

## Acknowledgments

This work is supported by the National Natural Science Foundation of China (11432010, 11502202, and 11672241) and Innovation Foundation for Doctor Dissertation of Northwestern Polytechnical University (CX201615). A large part of this work is carried out at University of Liverpool by the first author sponsored by China Scholarship Council.

## References

[1] J.D. Rouge, Space-based solar power as an opportunity for strategic security: phase 0 architecture feasibility study, Report to the Director, National Security Space Office, (2007) 1-42.
[2] H. Feingold, C. Carrington, Evaluation and comparison of space solar power concepts, Acta Astronautica, 53 (2003) 547-559.
[3] P.E. Glaser, Power from the sun: Its future, Science, 162 (1968) 857-861.
[4] W. Seboldt, M. Klimke, M. Leipold, N. Hanowski, European sail tower SPS concept, Acta Astronautica, 48 (2001) 785-792.
[5] S. Sasaki, K. Tanaka, K. Higuchi, N. Okuizumi, S. Kawasaki, N. Shinohara, K. Senda, K. Ishimura, A new concept of solar power satellite: Tethered-SPS, Acta Astronautica, 60 (2007) 153-165.
[6] C. Carrington, J. Fikes, M. Gerry, D. Perkinson, H. Feingold, J. Olds, The Abacus/Reflector and integrated symmetrical concentrator-Concepts for space solar power collection and transmission, in: 35th Intersociety Energy Conversion Engineering Conference and Exhibit, 2000, pp. 3067.
[7] J.C. Mankins, K. Nobuyuki, Space Solar Power: The first international assessment of space solar power: Opportunities, issues and potential pathways forward, International Academy of Astronautics (IAA)(Paris France), 2011.
[8] H. Matsumoto, K. Hashimoto, Report of the URSI Inter-Commission Working Group on SPS, URSI, Ghent, 2007.
[9] N. Takeichi, H. Ueno, M. Oda, Feasibility study of a solar power satellite system configured by formation flying, Acta Astronautica, 57 (2005) 698-706.
[10] S. Wu, K. Zhang, H. Peng, Z. Wu, G. Radice, Robust Optimal Sun-Pointing Control of a Large Solar Power Satellite, Acta Astronautica, 127 (2016) 226-234.
[11] I. McNally, D. Scheeres, G. Radice, Locating Large Solar Power Satellites in the Geosynchronous Laplace Plane, Journal of Guidance, Control, and Dynamics, 38 (2015) 489-505.
[12] B. Wie, C.M. Roithmayr, Attitude and orbit control of a very large geostationary solar power satellite, Journal of guidance, control, and dynamics, 28 (2005) 439-451.
[13] B. Wie, C.M. Roithmayr, Integrated orbit, attitude, and structural control systems design for space solar power satellites, National Aeronautics and Space Administration, Langley Research Center, 2001.
[14] Y. Liu, S. Wu, K. Zhang, Z. Wu, Gravitational orbit-attitude coupling dynamics of a large solar power satellite, Aerospace Science and Technology, 62 (2017) 46-54.
[15] H.A. Fujii, T. Watanabe, H. Kojima, K. Sekikawa, N. Kobayashi, Control of attitude and vibration of a tethered space solar power satellite, in: 2003 AIAA Guidance, Navigation and Control Conference and Exhibit, 2003.
[16] H.A. Fujii, Y. Sugimoto, T. Watanabe, T. Kusagaya, Tethered actuator for vibration control of space structures, Acta Astronautica, 117 (2015) 55-63.
[17] K. Ishimura, K. Higuchi, Coupling between structural deformation and attitude motion of large planar space structures suspended by multi-tethers, Acta Astronautica, 60 (2007) 691-710.
[18] K. Senda, T. Goto, Dynamics Simulation of Flexible Solar Power Satellite Using Geomagnetic Control, in: title The 24th Workshop on JAXA Astrodynamics and Flight Mechanics 2014, pp. 215.
[19] Q. Jin, J. Huang, J. Fan, Motion analysis and trajectory planning of solar tracking of a class of Space Solar Power Station, Solar Energy, 122 (2015) 239-248.
[20] Q. Jin, J. Huang, Moving analysis of Integrated Symmetrical Concectrated based on geosynchronous orbit, in: Fifth Asia International Symposium on Mechatronics (AISM 2015), 2015, pp. 1-5.
[21] J.G. De Jalon, E. Bayo, Kinematic and dynamic simulation of multibody systems: the real-time challenge, Springer Science & Business Media, 2012.
[22] J.G. de Jalon, J. Unda, A. Avello, Natural coordinates for the computer-analysis of multibody systems, Computer Methods in Applied Mechanics and Engineering, 56 (1986) 309-327.
[23] J.G. de Jalón, Twenty-five years of natural coordinates, Multibody System Dynamics, 18 (2007) 15-33.
[24] J. Zhao, Q. Tian, H. Hu, Deployment dynamics of a simplified spinning IKAROS solar sail via absolute coordinate based method, Acta Mechanica Sinica, 29 (2013) 132-142.
[25] C. Liu, Q. Tian, H. Hu, Dynamics of a large scale rigid–flexible multibody system composed of composite laminated plates, Multibody System Dynamics, 26 (2011) 283-305.
[26] C. Liu, Q. Tian, H. Hu, Dynamics and control of a spatial rigid-flexible multibody system with multiple cylindrical clearance joints, Mechanism and Machine Theory, 52 (2012) 106-129.

[27] S. Leyendecker, P. Betsch, P. Steinmann, Energy-conserving integration of constrained Hamiltonian systems–a comparison of approaches, Computational Mechanics, 33 (2004) 174-185.
[28] Y. Wang, S. Xu, Gravitational orbit-rotation coupling of a rigid satellite around a spheroid planet, Journal of Aerospace Engineering, 27 (2012) 140-150.
[29] O.A. Bauchau, A. Laulusa, Review of contemporary approaches for constraint enforcement in multibody systems, Journal of Computational and Nonlinear Dynamics, 3 (2008) 011005.
[30] L. Petzold, P. Lötstedt, Numerical solution of nonlinear differential equations with algebraic constraints II: Practical implications, SIAM Journal on Scientific and Statistical Computing, 7 (1986) 720-733.
[31] M. Arnold, O. Brüls, Convergence of the generalized-α scheme for constrained mechanical systems, Multibody System Dynamics, 18 (2007) 185-202.
[32] Y. Wei, Z. Deng, Q. Li, B. Wang, Projected Runge-Kutta methods for constrained Hamiltonian systems, Applied Mathematics and Mechanics, 37 (2016) 1077-1094.
[33] Y. Wei, Z. Deng, Y. Wang, Q. Li, An Improved Energy and Constraint Conserving Algorithm for Constrained Hamiltonian Systems, Journal of Computational and Theoretical Nanoscience, 13 (2016) 1055-1062.
[34] G. Sun, A simple way constructing symplectic Runge-Kutta methods, Journal of Computational Mathematics, 18 (2000) 61-68.
[35] F.L. Markley, J.L. Crassidis, Fundamentals of spacecraft attitude determination and control, Springer, New York, 2014.
[36] E. Hairer, S.P. Nrsett, G. Wanner, Solving Ordinary Differential Equations I: Nonstiff problems, Springer Verlag, 1993.
[37] A.K. Yadav, P. Gaur, Improved Self-Tuning Fuzzy Proportional-Integral-Derivative Versus Fuzzy-Adaptive Proportional-Integral-Derivative for Speed Control of Nonlinear Hybrid Electric Vehicles, Journal of Computational and Nonlinear Dynamics, 11 (2016).
[38] H.D. Curtis, Orbital mechanics for engineering students, Butterworth-Heinemann, 2013.